Volume 17 | Number 44 | 28 November 2015 | Pages 29397–30190

PCCP

Physical Chemistry Chemical Physics

www.rsc.org/pccp

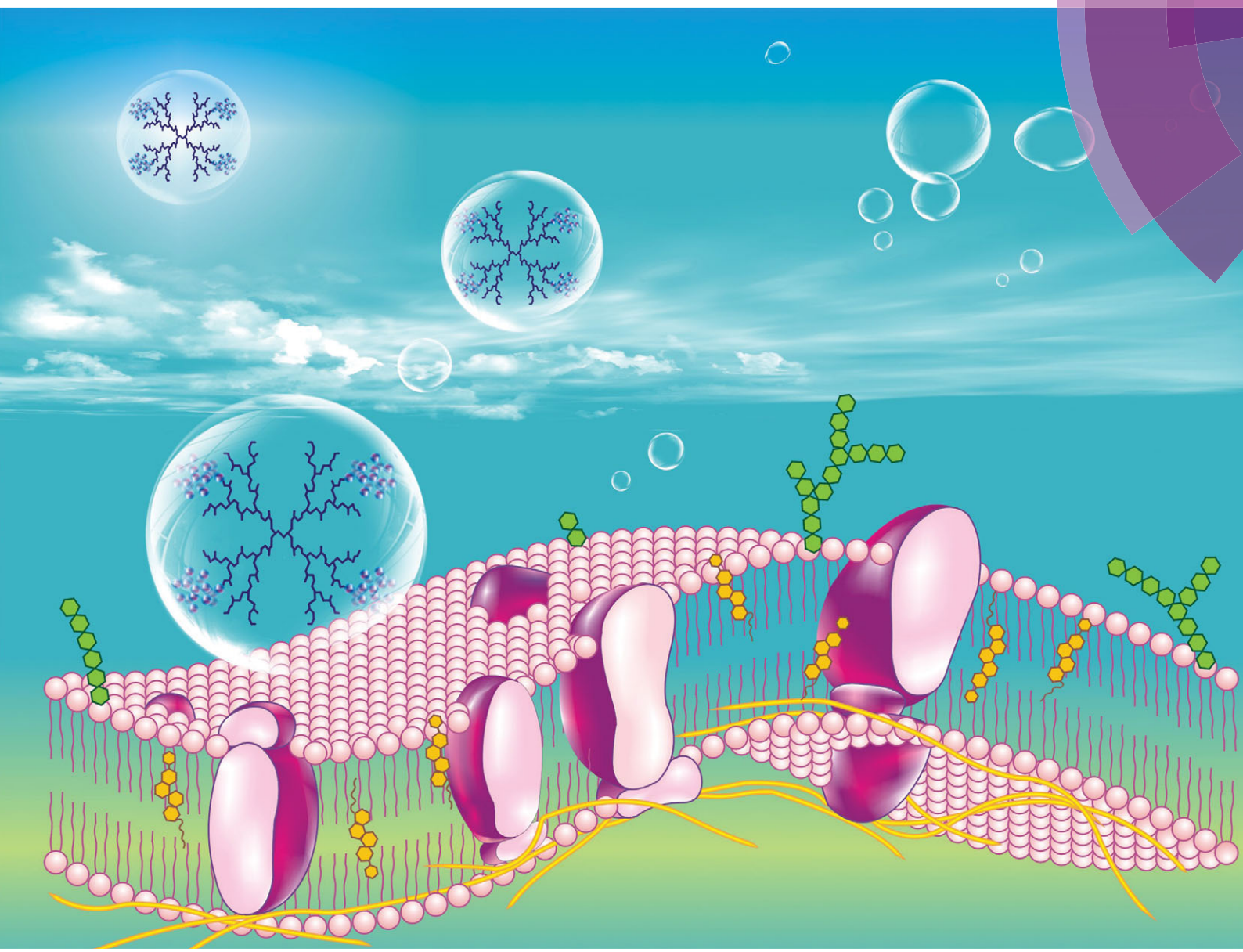

ISSN 1463-9076

ROYAL SOCIETY OF CHEMISTRY

PAPER

ZhiGuo Qu, Feng Xu *et al.*

Molecular analysis of interactions between a PAMAM dendrimer–paclitaxel conjugate and a biomembrane

PCCP

PAPER

View Article Online
View Journal | View Issue

Published on 27 July 2015. Downloaded by Xian Jiaotong University on 31/05/2016 08:36:03.

Cite this: *Phys. Chem. Chem. Phys.*, 2015, **17**, 29507

Molecular analysis of interactions between a PAMAM dendrimer–paclitaxel conjugate and a biomembrane†

XiaoCong He,[ab] Min Lin,[bc] TianJian Lu,[b] ZhiGuo Qu*[ab] and Feng Xu*[bc]

Received 17th April 2015,
Accepted 26th July 2015

DOI: 10.1039/c5cp02242h

www.rsc.org/pccp

Understanding the underlying mechanism of nanomedicine–biomembrane interactions is important for the design and optimization of payload delivery systems. This study investigates the interactions between polyamidoamine (PAMAM) dendrimer–paclitaxel conjugates and biomembranes using coarse-grained molecular dynamics simulations. We found that acidic conditions (*e.g.*, pH ~ 5) and membrane asymmetry can improve the conjugate penetration. Paclitaxel (PTX) distributions on a G4 PAMAM dendrimer can affect interactions *via* the penetration mechanism, although they have no significant effect on interactions *via* the adsorption mechanism. The random distribution of PTX can enhance the ability of PTX molecules to pass through asymmetric membranes. Furthermore, the penetration process becomes more difficult with increasing paclitaxel loading ratios. These results provide molecular insights into the precise translocation mechanism of dendrimer–drug conjugates and thus provide suggestions for drug design and delivery.

1. Introduction

Nanomedicine is finding widespread applications in almost every aspect of human health.[1–3] As an anti-cancer drug obtained from the bark of *Taxus brevifolia*, paclitaxel (PTX) has been widely used for the therapy of various cancers and sarcomas, including lung, ovarian, breast, head and neck cancers and Kaposi's sarcoma.[4–7] PTX molecules work by disrupting the normal microtubule dynamics in the cell division process and are thus particularly effective in killing cancer cells. However, the low aqueous solubility of PTX molecules (approximately 0.3 μg mL^{-1}) constrains their therapeutic applications.[8] In general, almost 40 percent of developed drug candidates are rejected by the pharmaceutical industry due to their low aqueous solubility and/or cell membrane permeability.[4] Therefore, one of the key challenges in nanomedicine is the design of carriers that efficiently deliver drugs with low aqueous solubility to target cell components.[9]

Among the various carriers identified thus far, polyamidoamine (PAMAM) dendrimers offer several advantages, including designable structures, high loading capability, monodispersity, biocompatibility and controlled release properties.[10,11] The drugs can interact with the dendrimers to form conjugates or complexes through either a covalent attachment *via* a selected linker or a non-covalent attachment *via* an electrostatic attraction, hydrophobic interaction or hydrogen bonding interaction.[11] Compared with a non-covalent attachment, the covalent bonding of PTX molecules to the dendrimer surface *via* a selected linker offers advantages in controlling drug release and drug targeting.[12] The PAMAM dendrimer and PTX molecule conjugate has become a promising nanomedicine for cancer therapy.[4]

In a drug delivery system, PAMAM dendrimer and PTX molecule conjugates should pass through the biomembrane barrier to reach cellular compartments and exert their therapeutic function.[13] Tremendous efforts have been made to explore the mechanisms of dendrimers entering cells by both direct penetration and endocytosis pathways.[14] However, the exact pathway through which dendrimers enter cells remains elusive. For instance, experimental studies have shown that the cytotoxicity of PAMAM dendrimer–PTX conjugates is 10 times higher than that of non-conjugated PTX molecules.[6] Although cell viability can be used to indicate drug cytotoxicity to cancer cells in experimental studies as an endpoint marker, it is difficult for experimental studies to determine an exact translocation mechanism. Therefore, understanding the detailed interactions between PAMAM dendrimer–PTX conjugates and biomembranes

[a] *Key Laboratory of Thermo-Fluid Science and Engineering of Ministry of Education, School of Energy and Power Engineering, Xi'an Jiaotong University, Xi'an 710049, P. R. China. E-mail: zgqu@mail.xjtu.edu.cn*
[b] *Bioinspired Engineering and Biomechanics Center (BEBC), Xi'an Jiaotong University, Xi'an 710049, P. R. China. E-mail: fengxu@mail.xjtu.edu.cn*
[c] *The Key Laboratory of Biomedical Information Engineering of Ministry of Education, School of Life Science and Technology, Xi'an Jiaotong University, Xi'an 710049, P. R. China*

† Electronic supplementary information (ESI) available. See DOI: 10.1039/c5cp02242h

Published on 27 July 2015. Downloaded by Xian Jiaotong University on 31/05/2016 08:36:03.

is necessary to reveal the potential mechanisms underlying the fundamental cellular events.

A biomembrane is a selectively permeable barrier to molecules and plays an important role in nanomedicine–biomembrane interactions.[15] In many natural membranes, the lipid compositions of two membrane leaflets are different, such as in human erythrocyte membranes.[16] In our previous study, we found that membrane asymmetry can affect the fundamental cellular events, such as cellular uptake.[17] Therefore, considering membrane asymmetry in the nanomedicine–biomembrane interaction is necessary.

This work included coarse-grained molecular dynamics (CGMD) simulations to investigate the interactions between PAMAM

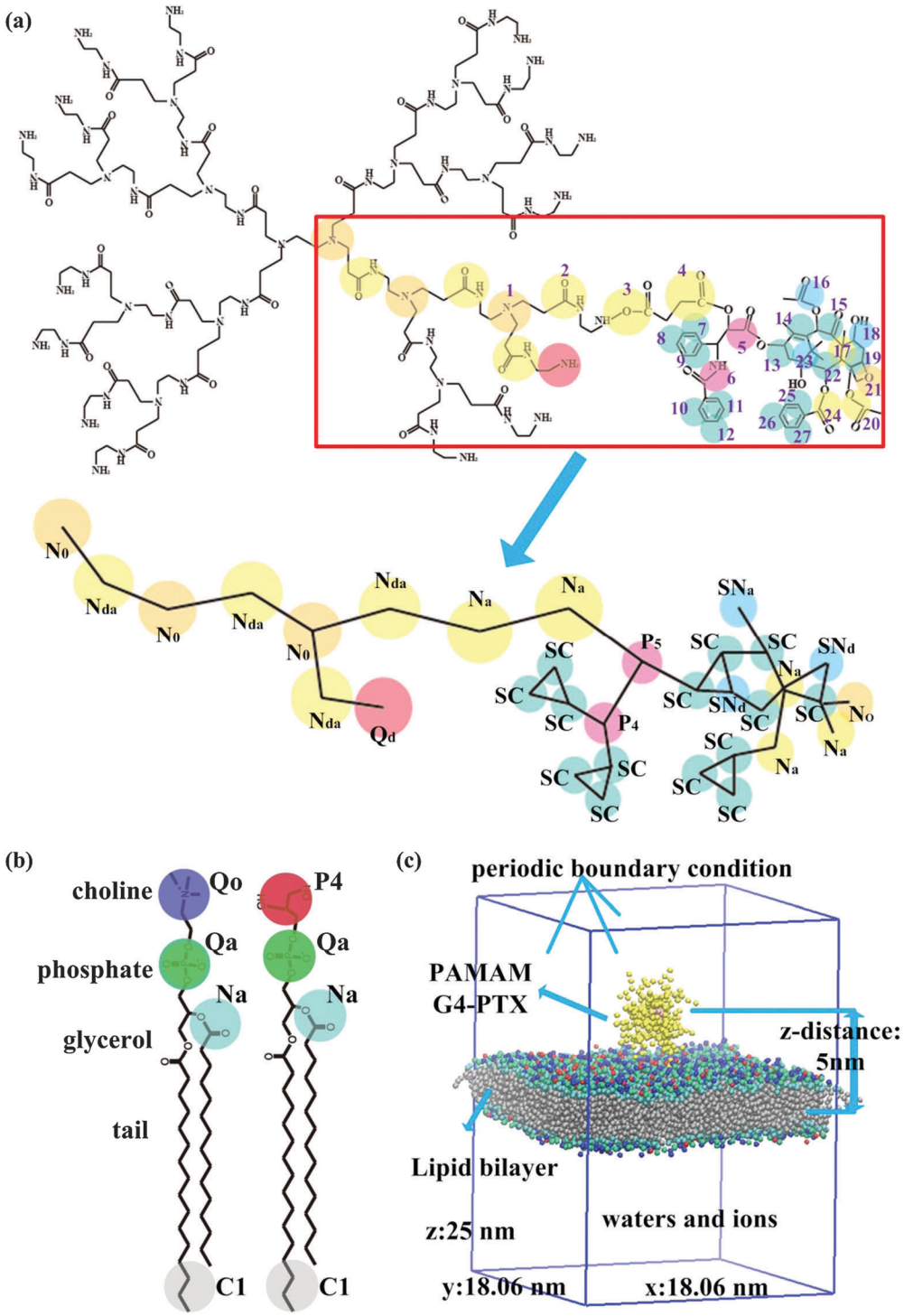

Fig. 1 Structures of the PAMAM dendrimer–PTX conjugate, lipid molecules and the simulation box. Mapping of the G2 PAMAM dendrimer–PTX conjugate (a) and DPPC, DPPG lipid molecules (b) based on the Martini force field. (c) The detailed information on the simulation box.

 This journal is © the Owner Societies 2015

Published on 27 July 2015. Downloaded by Xian Jiaotong University on 31/05/2016 08:36:03.

dendrimer–PTX conjugates and biomembranes. We analyzed the effects of PTX molecule distribution at the dendrimer surface and the PTX molecule loading ratio on the interactions. In addition, the competitive relationship between the dendrimer properties and the PTX properties in the interactions is shown. Our study provides deep insights into the mechanism of interactions between nanomedicine and biomembranes at the molecular level, which can impact nanomedicine design and targeted drug delivery.

2. Model and methods

CGMD simulations are used to investigate the nanomedicine–biomembrane interactions because they present larger spatial and temporal scales compared with all-atom molecular dynamics simulations.[18–20] As a typical CG force field, the Martini force field developed by Marrink *et al.*[21] is used to simulate biological systems (such as lipids, proteins, and genes). Four types of particles (polar (P), apolar (C), nonpolar (N), and charged (Q)) are defined, and four heavy atoms are generally represented by one CG particle. Thus, the effective time is four times faster than that in an all-atom model.[22]

In a physiological environment, the PAMAM dendrimer consists of a primary amine group at each branch end and a tertiary amine group at each branching point. The atomic structure and CG mapping, based on the Martini force field of a PAMAM dendrimer (generation two: G2), are shown in Fig. 1a. We adopted this coarse-grained model of a PAMAM dendrimer from the study of Lee *et al.*[23] The tertiary amine group and the primary amine group are coarse-grained to particles N_0 and N_{da}, respectively. The surface groups of the dendrimer are represented by Q_d. Each CG structure of the G4 PAMAM dendrimer contains 250 CG particles and 64 positive charges. The parameters of bonded interactions (bond and angle potential energy) and non-bonded interactions (Coulombic energy and L-J potential energy) are listed in Table 1. To equilibrate the CG dendrimer model, long simulations (1 μs) were performed in the solvents.[24] The gyration radius of the G4 dendrimer is 1.98 in the physiological environment, which coincides with previous studies (Table 2).[24–26]

The experimental study of Khandare *et al.*[6] showed the structure of the PAMAM dendrimer–PTX conjugate, where the PTX molecule and the PAMAM G4 hydroxyl-terminal dendrimer were bonded to two sides of the linker (small molecule: succinic acid) to form the PAMAM dendrimer–PTX conjugate. We used the above conjugate structure in this study; the atomic and coarse-grained structures of the conjugate are shown in Fig. 1. We used the coarse-grained PTX molecule model from the study of Peng *et al.*,[27] and the detailed parameters of bonded interactions are shown in Table 3. To equilibrate the CG conjugate models, long simulations (1 μs) were performed in the solvents for each conjugate.

Table 2 PAMAM dendrimer radii of gyration (R_g) under different pH conditions in equilibrium compared with references

pH	Maiti *et al.*[25]	Ma *et al.*[24]	Lee *et al.*[26]	Our simulation (G4)
5	1.9	2.22	2.99	2.52
7	1.7	1.81	2.67	1.98
10	1.68	1.69	1.48	1.70

Table 1 Detailed description of the PAMAM dendrimer model and the lipid model in the Martini CG force field

Interaction	Type	Equation	Parameter
PAMAM dendrimer model			
Non-bonded interactions	LJ potential	$U_{LJ}(r) = 4\varepsilon_{ij}\left[\left(\frac{\sigma_{ij}}{r}\right)^{12} - \left(\frac{\sigma_{ij}}{r}\right)^{6}\right]$	σ_{ij} = 0.47 nm
	Coulombic energy	$U_{el}(r) = \frac{q_i q_j}{4\pi\varepsilon_0\varepsilon_r r}$	ε_r = 15
Bonded interactions	Bond potential energy	$V_b = \frac{1}{2}K_b(d_{ij} - d_b)^2$	d_b = 0.5 nm K_b = 1250 (kJ mol^{-1} nm^{-2})
	Angle potential energy	$V_a = \frac{1}{2}K_a[\cos(\theta_{ijk}) - \cos(\theta_a)]^2$	θ_{a1} = 180° K_{a1} = 150 (kJ mol^{-1} rad^{-2}); θ_{a2} = 120° K_{a2} = 150 (kJ mol^{-1} rad^{-2})
Lipid model			
Non-bonded interactions	LJ potential	$U_{LJ}(r) = 4\varepsilon_{ij}\left[\left(\frac{\sigma_{ij}}{r}\right)^{12} - \left(\frac{\sigma_{ij}}{r}\right)^{6}\right]$	σ_{ij} = 0.47 nm
	Coulombic energy	$U_{el}(r) = \frac{q_i q_j}{4\pi\varepsilon_0\varepsilon_r r}$	ε_r = 15
Bonded interactions	Bond potential energy	$V_b = \frac{1}{2}K_b(d_{ij} - d_b)^2$	d_b = 0.47 nm K_b = 1250 (kJ mol^{-1} nm^{-2})
	Angle potential energy	$V_a = \frac{1}{2}K_a[\cos(\theta_{ijk}) - \cos(\theta_a)]^2$	θ_a = 180° K_a = 150 (kJ mol^{-1} rad^{-2})

Published on 27 July 2015. Downloaded by Xian Jiaotong University on 31/05/2016 08:36:03.

Table 3 Detailed description of bonded interactions for the CG PTX molecule model in the Martini CG force field

i	j	Bond length L (nm)	Force constant K (kJ mol^{-1} nm^{-2})	i	j	k	Bond angle θ (°)	Force constant K (kJ mol^{-1} rad^{-2})
1	2	0.5	1250	1	2	3	180	150
2	3	0.5	1250	2	3	4	149	100
3	4	0.340	7500	3	4	5	97	100
4	5	0.325	7500	4	5	6	91	100
5	6	0.258	7500	4	5	13	154	100
6	7	0.353	7500	5	6	7	107	100
6	10	0.318	7500	5	6	10	75	100
5	13	0.198	7500	5	13	14	80	100
13	14	0.227	7500	5	13	23	158	100
7	8	0.270	1000	6	7	8	173	100
7	9	0.270	1000	6	7	9	109	100
8	9	0.270	1000	6	10	11	143	100
10	11	0.270	1000	6	10	12	105	100
10	12	0.270	1000	13	14	22	95	100
11	12	0.270	1000	13	14	15	127	100
13	23	0.223	7500	13	22	24	85	100
14	23	0.342	7500	14	23	22	60	100
14	15	0.382	7500	14	15	16	52	100
15	16	0.519	7500	14	15	17	36	100
15	17	0.609	7500	15	17	22	53	100
17	18	0.578	7500	15	17	18	85	100
18	19	0.289	7500	15	17	19	48	100
17	19	0.469	7500	16	17	24	31	100
17	22	0.138	7500	17	19	21	120	100
19	20	0.349	7500	18	19	20	115	100
19	21	0.249	7500	18	19	21	121	100
22	24	0.368	7500	18	17	19	30	100
22	23	0.369	7500	22	18	19	54	100
24	25	0.238	7500	22	19	20	105	100
25	26	0.270	1000	22	24	25	125	100
25	27	0.270	1000	23	22	13	75	100
26	27	0.270	1000	23	22	24	96	100
				24	25	26	128	100
				24	25	27	165	100

Two types of lipid molecules are used in our simulations, including dipalmitoylphosphatidylcholine (DPPC) and dipalmitoylphosphatidylglycerol (DPPG). The lipid molecule consists of a choline group, a phosphate group and a glycerol group for its head group and two carbon tails (Fig. 1c). The mapping of lipids based on the Martini force field[21] is shown in Fig. 1c: the choline groups of lipids are represented by the CG beads Qo and P4 for DPPC and DPPG, respectively. The phosphate group, the glycerol group and the carbon tails of all lipids are represented by Qa, Na and C1, respectively. The parameters of bonded interactions (bond and angle potential energy) and non-bonded interactions (L-J potential energy and Coulombic energy) for lipids in the Martini CG force field[21] are shown in Table 1. The DPPC : DPPG ratio is 3 : 1 for a symmetric membrane, which is based on the membrane charge density.[28] However, numerous studies[15,29,30] have shown that the membranes of most eukaryotic cells are asymmetric. For instance, negatively charged lipids may be located in the inner membrane leaflet, inducing significant differences in charge distribution between the two membrane leaflets.[29] The percentage of negatively charged lipids in the inner leaflet among total membrane lipids ranges from 6%[31] to 33%[15] in previous studies. Therefore, to maintain the same charge density as the symmetric membrane above (PG: 25%), we simulated the asymmetric membrane as follows: the outer membrane leaflet is DPPC only and the ratio of DPPC : DPPG is 1 : 1 for the inner membrane leaflet (Table 4). Each membrane containing 1040 CG lipid molecules was equilibrated in the solvent system for 200 ns with the *NPT* ensemble.

Table 4 Parameters of simulation systems

System	pH	Membrane	Membrane charge	NP	NP charge	Ions
1	5	Symmetric[a]	260−	G4-1PTX	125+	135 Na^+
2	5	Asymmetric[b]	260−	G4-1PTX	125+	135 Na^+
3	7	Symmetric	260−	G4-1PTX	63+	197 Na^+
4	7	Asymmetric	260−	G4-1PTX	63+	197 Na^+
5	10	Symmetric	260−	G4-1PTX	0	260 Na^+
6	10	Asymmetric	260−	G4-1PTX	0	260 Na^+
7	7	Asymmetric	260−	G4-4PTX	60+	200 Na^+
8	7	Asymmetric	260−	G4-8PTX	56+	204 Na^+
9	7	Asymmetric	260−	G4-16PTX	48+	212 Na^+

[a] Symmetric membrane: DPPC : DPPG = 780 : 260. [b] Asymmetric membrane: outer leaflet DPPC = 520; inner leaflet DPPC : DPPG = 260 : 260.

In the initial state, the PAMAM dendrimer–PTX conjugate was placed 6 nm above the membrane (center of mass separation distance in the *z*-direction (*z*-distance)) (Fig. 1d). The box size in the initial state is 18.06 × 18.06 × 25 nm. The periodic boundary conditions were used in all simulations. After energy minimization, a constrained simulation (force constant: 1000 kJ mol^{-1} nm^{-2}) was performed to constrain the membrane and the conjugate in order to equilibrate water and ions. Long MD simulations (960 ns) were then performed to ensure that the systems achieved an equilibrated state. The *NPT* ensemble was used in the simulations: Berendsen thermostat and pressure couplings were used to maintain constant system temperature (323 K) and pressure (1 bar).[32] A particle mesh Ewald summation (PME) method[33] was used to chart electrostatic interactions, and a cutoff of 1.2 nm was used for van der Waals (vdW) interactions. To reduce the cutoff noise, the L-J potential was smoothly shifted to zero between 0.9 and 1.2 nm. For the potential of mean force (PMF) calculation, the umbrella sampling[34] and weighted histogram analysis[35] methods were used. Initialized conformations were assessed with a 0.2 nm step size. A long run of 360 ns was performed in each sample, and the last 240 ns run was used for data analysis. GROMACS 4.5.4 package[36] and Visual Molecular Dynamics (VMD) 1.9 software[37] were used to perform all simulations and present the results.

3. Results and discussion

3.1 Effect of pH

Previous studies have demonstrated that pH conditions can affect the effective interaction between pH-sensitive dendrimers and biomembranes.[38] The pH environment can be different in biological systems, for instance, the pH value is near 5 in endosomal vesicles and near 7 in the cytoplasm. Under acidic conditions (pH ~ 5), all primary amine groups and tertiary amines are protonated (positively charged) (Fig. 2a). At physiological pH (~7), only the surface monomers are protonated (Fig. 2b). Under high pH conditions (~10), no amines are

 This journal is © the Owner Societies 2015

Published on 27 July 2015. Downloaded by Xian Jiaotong University on 31/05/2016 08:36:03.

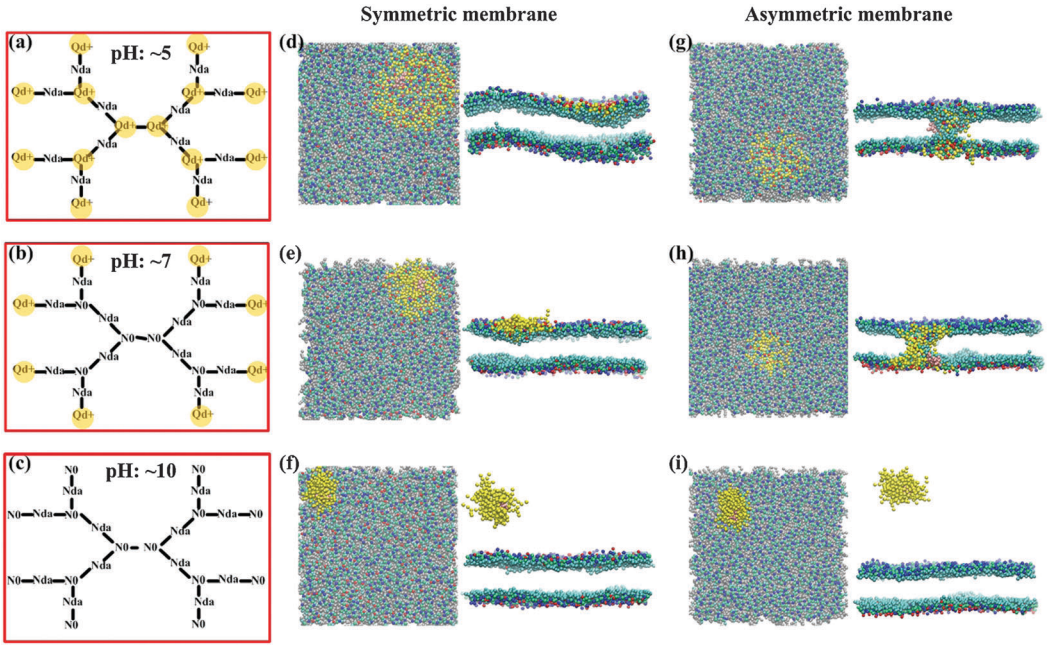

Fig. 2 Snapshots of interactions between conjugates and biomembranes under different pH conditions in an equilibrated state. Left row: schematics of the PAMAM dendrimer CG structure under acidic (a), physiological (b) and alkaline (c) conditions. Middle row: snapshots of conjugates interacting with symmetric membranes under acidic (d), physiological (e) and alkaline (f) conditions in equilibrated states. Right row: snapshots of conjugates interacting with asymmetric membranes under acidic (g), physiological (h) and alkaline (i) conditions in equilibrated states.

protonated and the dendrimer is neutrally charged (Fig. 2c).[38] Thus, three conjugates (pH ~5, ~7, and ~10) interacting with symmetric and asymmetric membranes were simulated to obtain insights into the effect of pH conditions on conjugate–biomembrane interactions.

In assessing the conjugate–symmetric membrane interactions under different pH conditions, snapshots in equilibrated states (Fig. 2d–f) show that the conjugate tightly adsorbs onto the membrane and induces a negative curvature in the membrane under low pH conditions (~5). This phenomenon is different from results of a previous study[38] that showed a G4 dendrimer penetrating into the lipid bilayer under acidic conditions (pH ~5). This difference is attributed to the dendrimer concentration (ratio of dendrimer and lipid) that was verified to affect the interaction – a higher concentration positively affects the dendrimer insertion into the membrane.[22] Under physiological conditions (pH ~7), the conjugate simply rests on the membrane surface. Furthermore, we observed that the conjugate under acidic conditions was more expansive than that under physiological conditions (top views). Because the conjugate under low pH conditions is more positively charged than that under physiological conditions, the enhanced electrostatic attraction leads to tighter adsorption and membrane curvatures. Under high pH conditions (pH ~10), the conjugate remains far above the membrane due to its hydrophilic property and the absence of charges.

However, different phenomena were observed for asymmetric membrane cases where the conjugate inserts into the lipid bilayer under acidic and physiological conditions (Fig. 2g–i). These results can be attributed to the electrostatic interactions between the conjugate and the DPPG lipids in the inner membrane leaflet, which have been proven to play a major role in the penetration process.[17] The above results indicate that the pH environment significantly affects the interactions between conjugates and biomembranes based on their pH sensitivity, which was also shown in experimental studies.[39]

Furthermore, it was observed that the PTX molecule within the conjugate can pass through the membrane from the outer leaflet to the inner leaflet under a physiological pH condition in equilibrium (Fig. 2h). To understand this, we checked the conjugate penetration process (Fig. 3). The conjugate rapidly adsorbs onto the membrane and induces a membrane curvature within 30 ns, primarily because of electrostatic attraction. At approximately 78 ns, the dendrimer inserts into the lipid bilayer, while the PTX molecule remains on the outer membrane leaflet. The time required for the PTX molecule to arrive at the membrane center and the inner membrane leaflet is 90 ns and 150 ns, respectively. Finally, the PTX molecule remains in the inner membrane leaflet in an equilibrated state (960 ns). In this process, the hydrophobic PTX molecule prefers to stay at the membrane center to interact with the carbon tails of the lipids. However, the dendrimer branch linked to the PTX molecule is hydrophilic. The dendrimers exert a dominant role in this situation, which brings the PTX molecule to the lipid head groups. An experimental study[6] investigating the cellular localization of the dendrimer–paclitaxel conjugate showed that a PAMAM dendrimer can enhance paclitaxel penetration into cancer cells and showed a significantly higher toxicity to A2780 human ovarian carcinoma cells (the drug dose required to kill 50% of the cells was ten times lower) than the free paclitaxel drug.

Published on 27 July 2015. Downloaded by Xian Jiaotong University on 31/05/2016 08:36:03.

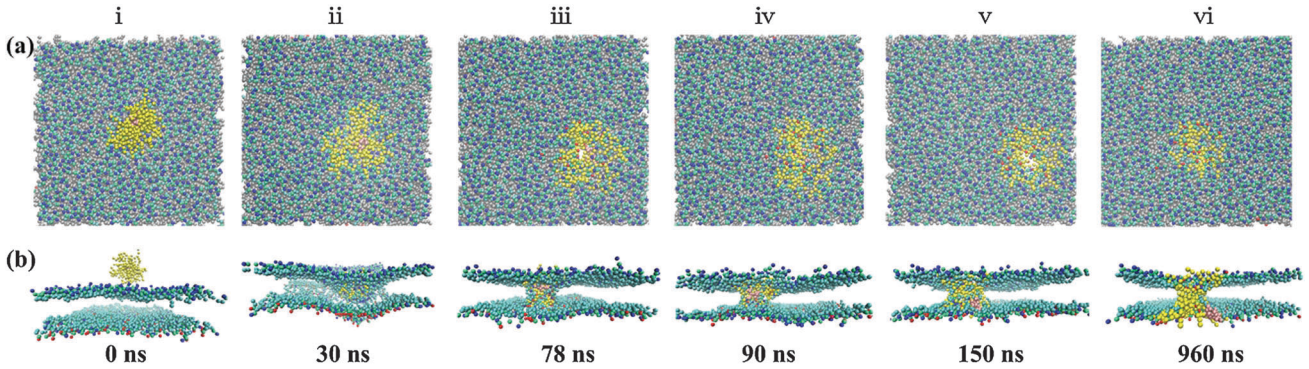

Fig. 3 Time sequence of snapshots of interactions between conjugates and asymmetric membranes under physiological conditions. (a) Top view and (b) side view.

The quantified *z*-distance (the center of mass separation distance on the *z* axis) between the PTX molecule and the membrane in the penetration process was analyzed to further understand the above interaction (pH ~ 7) (Fig. 4a). The fast drop near 30 ns is due to the membrane curvature (Fig. 3b-ii); the subsequent slow drop indicates the PTX molecule penetration. In combining the top and side views of the snapshots, we observed that a hydrophilic hole forms in the membrane during the conjugate insertion (Fig. 4b). Radial distribution functions (RDFs) of the PAMAM dendrimer and each lipid group with respect to the PTX molecule are shown in Fig. 4c. All RDFs were averaged over the last 200 ns. There were two high peaks at approximately 1 nm and 3 nm in the RDF of the PAMAM dendrimer with respect to the PTX molecule (purple line in Fig. 4c) because the inserted dendrimer remains

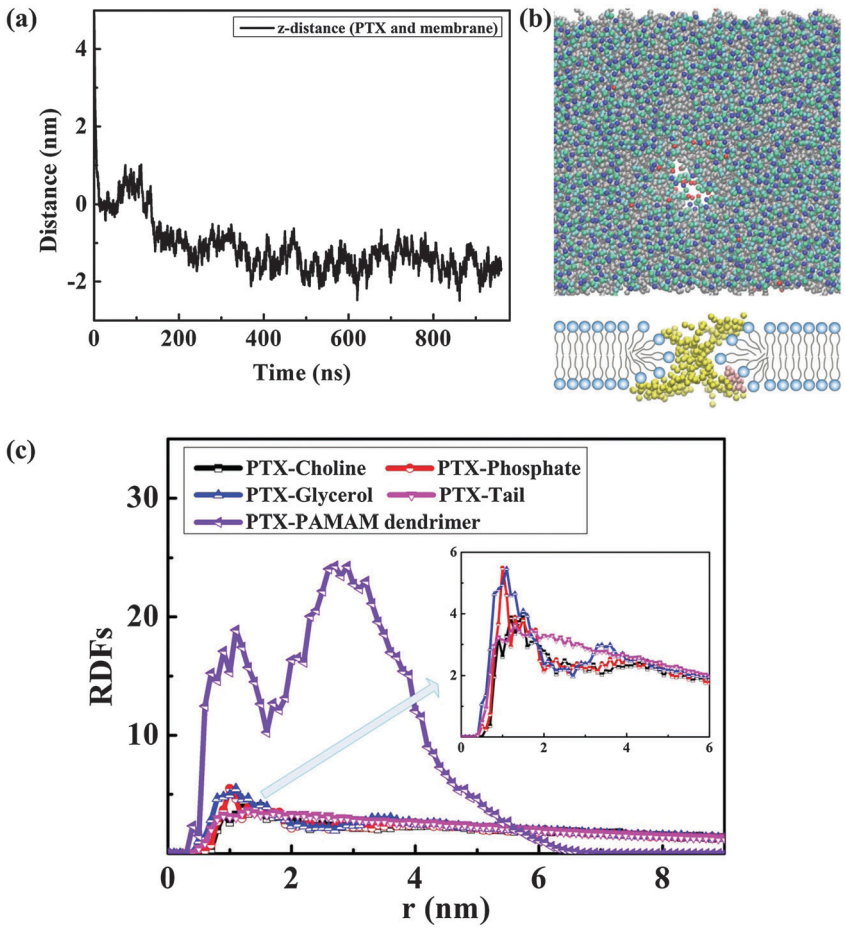

Fig. 4 Penetration mechanism of conjugate–membrane interactions. (a) The *z*-distance (between PTX molecule and membrane), (b) the hole formation mechanism and (c) RDFs (PTX molecule with respect to other groups) of interactions between conjugates and asymmetric membranes under physiological conditions.

 This journal is © the Owner Societies 2015

Published on 27 July 2015. Downloaded by Xian Jiaotong University on 31/05/2016 08:36:03.

separate at the outer and inner membrane leaflets, which was also shown in previous simulation studies.[9,23] The second-highest peak was observed in the phosphate and glycerol groups (red and blue lines in Fig. 4c). Two other peaks were observed in the choline groups (black line in Fig. 4c) and tail groups (pink line in Fig. 4c). These results indicate that the PTX molecule adsorbs at the bottom of the lipid head groups. This phenomenon is similar to the interaction between positively charged peptides and biomembranes.[40] This can be attributed to the fact that the positively charged PAMAM dendrimer repels positively charged choline groups and attracts negatively charged phosphate groups. The PAMAM dendrimer branches surrounding the PTX molecule play a dominant role, even though the PTX molecule prefers to interact with lipid carbon tails.

3.2 The effect of PTX molecule distribution

Nanoparticle shapes and sizes are the two most important factors in nanomaterial–biomembrane interactions.[41,42] The PTX molecule distribution on the polymer surface can affect the shape and size of the polymer–drug conjugate.[27] To understand the effect of PTX molecule distribution on these interactions, we simulated conjugates with clustered or random distributions of four PTX molecules interacting with either symmetric (Fig. 5) or asymmetric membranes (Fig. 6). As to interactions with symmetric membranes, the results show that conjugates adsorb onto the membranes in both clustered and random distributions (Fig. 5a). This result can also be confirmed by the *z*-distances between the conjugates and the symmetric membranes (Fig. 5b). The red and black lines almost overlap with each other, indicating that the PTX molecule distribution has no significant effect on conjugate–symmetric membrane interactions.

However, as to the case of asymmetric membranes, the results are different (Fig. 6a). With a clustered distribution of PTX molecules, the conjugate inserts into the symmetric membrane, while most PTX molecules gather at the membrane center. As to the random distribution, the conjugate inserts into the membrane, but one in four PTX molecules penetrates through the membrane to arrive at the inner membrane leaflet. To improve the statistics, we repeated the above interaction (four PTX molecules, random distribution) four more times. The snapshots in the equilibrated states and the *z*-distances between the PTX molecules and membranes are shown in the ESI† (Fig. S1). In the other four attempts, one in four PTX molecules penetrated through the membrane in three of the attempts (Fig. S1a–c, ESI†). Only one attempt showed a single PTX molecule going to the outer membrane leaflet (Fig. S1d, ESI†).

To further assess the interactions with asymmetric membranes, we quantified the *z*-distances between the PTX molecules with clustered/random distributions and the G4 PAMAM dendrimer (Fig. 6b and c). The *z*-distances ranged from −1.5 to 1.5 nm at the initial moment for a clustered distribution (Fig. 6b), while they were still within this range in the equilibrium state. However, when the PTX molecules are in a random distribution, the *z*-distances are almost at 0 nm at the initial moment (Fig. 6c). However, three PTX molecules are still near the dendrimer center, while the fourth PTX molecule separates far away from the dendrimer in the equilibrated state (PTX4 in Fig. 6c). These results indicate that the random distribution of PTX can enhance the chance of PTX molecules passing through the asymmetric membrane.

To further understand the differences in interactions with random/clustered PTX distributions, we calculated the potential of mean force (PMF) as a means of understanding the energetic costs of the interactions (Fig. 6e). The value of the PMFs for interactions with both random and clustered PTX distributions decreased at the onset due to the electrostatic attractions. They eventually reach a local minimum free energy value near 0.5 nm in the *z*-distance between the conjugate and the membrane, which are the preferred positions of the conjugates. Furthermore, compared with these two PMF curves, the PMF curve with clustered PTX distributions has a narrower shape, which indicates that the probability of the conjugate finding the preferred position is higher.[28] However, in the case of random PTX distributions, the PMF profile changes slightly around the preferred position. This result indicates that bringing the PTX molecules to the lipid head groups of the inner leaflet of the dendrimer branches is a difficult process because the PTX molecule is hydrophobic and thus prefers to stay within the lipid tails.

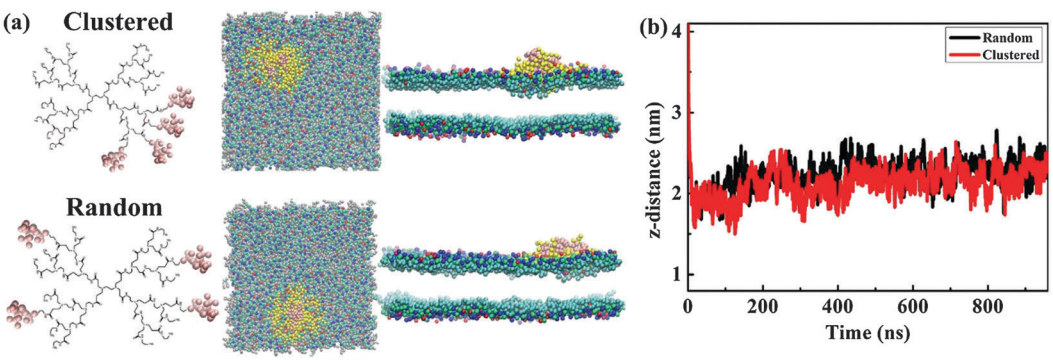

Fig. 5 Interactions between symmetric membranes and conjugates with different PTX molecule distributions. (a) Snapshots of conjugates with clustered and random PTX molecule distributions interacting with symmetric membranes in equilibrated states. (b) The *z*-distance between conjugates and symmetric membranes.

Published on 27 July 2015. Downloaded by Xian Jiaotong University on 31/05/2016 08:36:03.

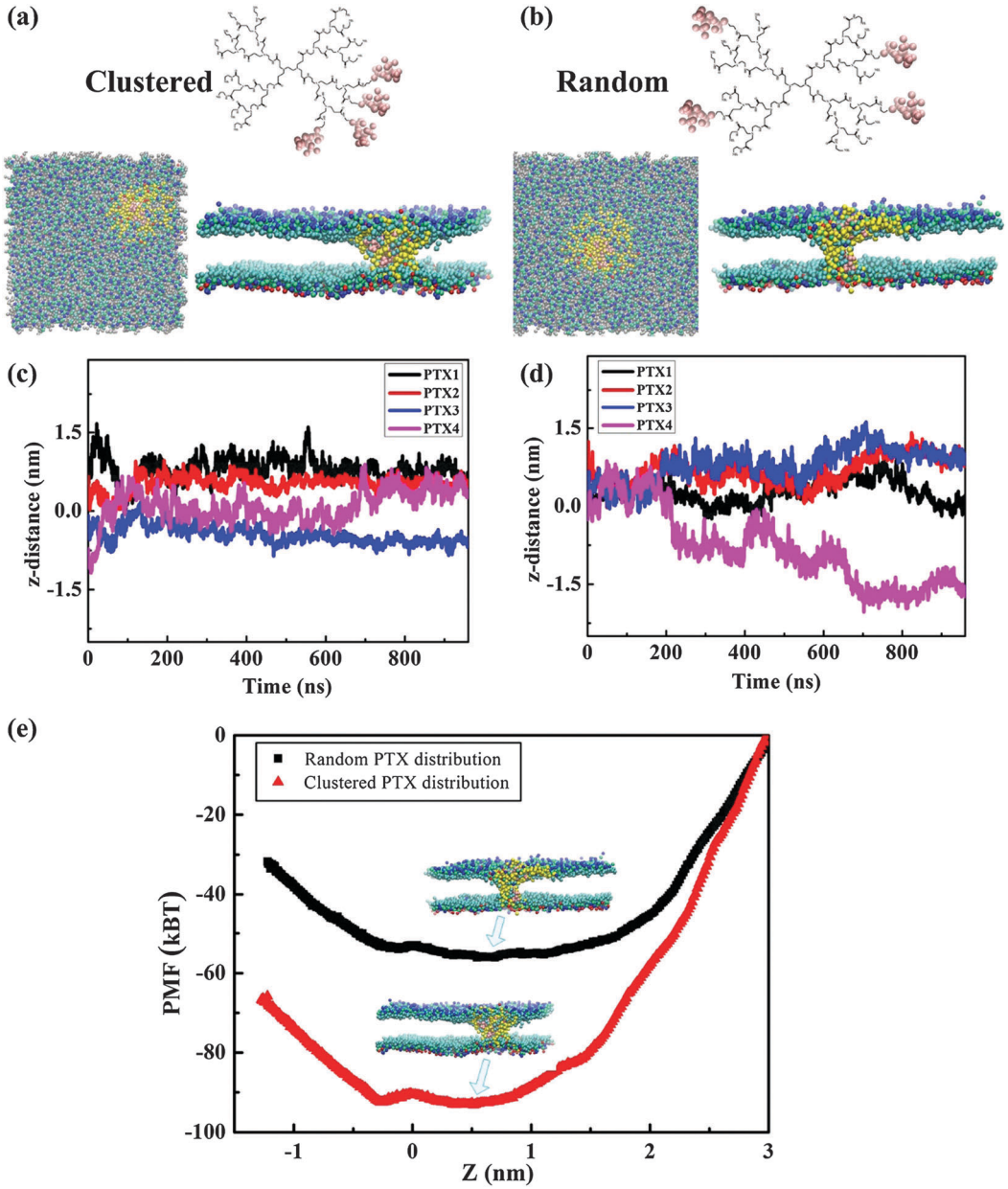

Fig. 6 Effects of different PTX molecule distributions on the interactions. Snapshots of conjugates with (a) clustered and (b) random PTX molecule distributions interacting with asymmetric membranes in equilibrated states. (c and d) The z-distance between PTX molecules and G4 PAMAM dendrimer: PTX molecules with clustered (b) and random (c) distributions. (e) PMF of interactions between conjugates with clustered/random PTX molecule distributions and asymmetric membranes.

3.3 The effect of the PTX molecule loading ratios

Achieving a high drug loading ratio is one of the most important goals in nanoparticle design and drug delivery,[11] However, existing evidence has shown that attaching a large number of drugs results in conjugate insolubility, thus affecting the interactions with the cell membrane.[43] For instance, complexes become insoluble when attaching five or more ibuprofen molecules to G4 PAMAM dendrimers.[44] To understand the effect of PTX molecule loading ratios on interactions, four conjugates were designed with different PTX molecule loading ratios (one, four, eight and 16 PTX molecules), and their interactions with asymmetric membranes were investigated (Fig. 7).

As to the interaction with one PTX molecule, the PTX molecule passes through the membrane (Fig. 7a), and one of the four PTX molecules arrives at the inner membrane leaflet for the interaction with four PTX molecules (Fig. 7b). However, in the cases of eight and 16 PTX molecules, all of the PTX molecules gather at the membrane center (Fig. 7c and d). These results indicate that conjugate hydrophobicity increases with increasing PTX molecule loading ratios. The PTX molecules prefer to stay within lipid carbon tails due to their poor water solubility. The hydrophobic

 This journal is © the Owner Societies 2015

Published on 27 July 2015. Downloaded by Xian Jiaotong University on 31/05/2016 08:36:03.

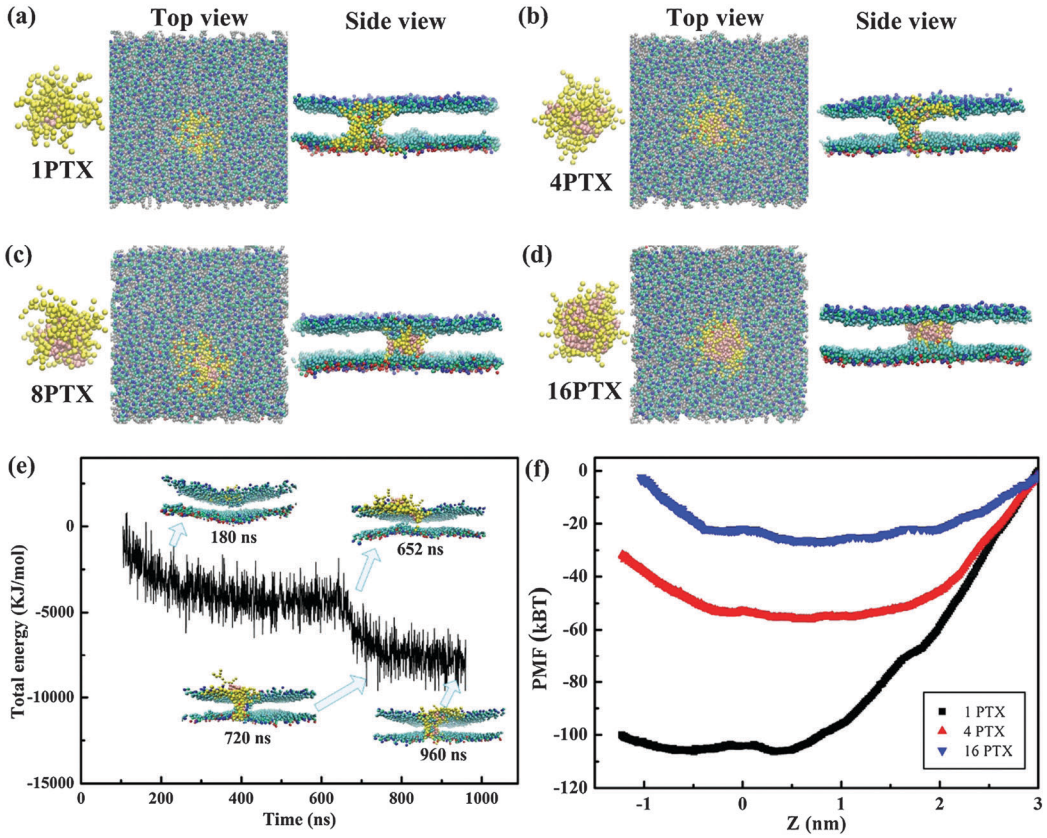

Fig. 7 Effects of different drug loading ratios on the interactions. Snapshots of interactions between asymmetric membranes and conjugates with different drug loading ratios in equilibrated states: (a–d) 1, 4, 8, and 16 PTX molecules, respectively. (e) Time evolution of system's total energy of interactions (four PTX molecules, random PTX molecule distribution). (f) The PMF of interactions between conjugates with different drug loading ratios and asymmetric membranes.

property of the conjugate dominates the interaction in these situations. However, an experimental study showed that PEG chains can improve the solubility.[45] For instance, PEGylated dendrimers can conjugate a maximum of 32 ibuprofen molecules.[43]

To further understand the effect of PTX molecule loading ratios, we quantified the time evolution of the system's total energy of interactions (four PTX molecules, random distribution) with an asymmetric membrane (Fig. 7e). We observed two declines in total energy during the process. The first involves the adsorption of the conjugate onto the membrane, while the second small decline in energy can be attributed to the penetration of the conjugate. Based on the representative snapshots (Fig. 7e), we observed that the time for conjugate insertion into the membrane was approximately 652 ns, which is much slower (~600 ns delay) than the interaction between a conjugate with one PTX molecule and an asymmetric membrane (Fig. 3). Furthermore, the PFMs of interaction between conjugates with different drug loading ratios and asymmetric membranes showed that the preferred positions for conjugates are 0.32 nm, 0.54 nm and 0.73 nm in the *z*-direction between the conjugate and the membrane for drug loading ratios of 1PTX, 4PTX and 16 PTX, respectively (Fig. 7f). These results indicate that penetration becomes more difficult with increasing PTX molecule loading ratios because of the decrease in the positively charged conjugate. A previous study showed the importance of electrostatic interactions in the dendrimer insertion process: the electrostatic potential energy decrease was 50 times greater than the potential energy decrease in the interactions.[38]

In addition to the factors mentioned above, different generations of PAMAM dendrimers can significantly affect the interactions between nanoparticles and biomembranes.[17,22,46] For instance, a previous study[17] showed that compared with a G4 PAMAM dendrimer a G5 dendrimer creates more perturbation to the asymmetric membrane and induces transient pore formation. As to high-generation PAMAM dendrimers, another study[46] showed that G7, G8, and G9 dendrimers changed their configurations very slightly during the interaction, indicating that these high-generation dendrimers can be regarded as rigid nanoparticles. In addition, membrane wrapping was observed in high-generation dendrimers when the dendrimer interacted with a defective membrane with pores.

All simulations in this work were conducted under the framework of the Martini force field. As any other model, the Martini model has limitations. The Martini model has been proven to break down in the case of pore formation in the lipid bilayer.[47] Bennett and Tieleman observed pore formation and membrane structure defects in an atomistic simulation, even

Published on 27 July 2015. Downloaded by Xian Jiaotong University on 31/05/2016 08:36:03.

though no pores were formed with the Martini model in their study.[48] However, this work focused on analyzing the competitive relationship between dendrimer properties and PTX properties in the interactions. Therefore, although limitations exist in the Martini model, our simulations provide insights into the translocation mechanism of conjugates and offer suggestions for drug design and delivery.

4. Conclusions

In this study, the interactions between PAMAM dendrimer–PTX conjugates and biomembranes were investigated through CGMD simulations. We discussed the interaction mechanism, the effect of pH conditions, the PTX molecule distributions and the PTX molecule loading ratios on these interactions to indicate the competitive relationship between dendrimer properties and PTX properties in the interactions. It was found that acidic conditions (*e.g.*, pH $\sim$ 5) and membrane asymmetry can improve conjugate penetration. The paclitaxel (PTX) distribution on G4 PAMAM dendrimers can affect interactions with the penetration mechanism, although these distributions exert no significant effect on interactions with the adsorption mechanism. A random distribution of PTX can enhance the chance of PTX molecules passing through asymmetric membranes. However, the penetration process becomes more difficult with increasing paclitaxel loading ratios. These results provide molecular insights into the mechanism underlying the interactions between dendrimer–drug conjugates and biomembranes, as well as suggestions for nanomedicine design and drug delivery.

Author contributions

ZG.Q., F.X. and TJ.L. conceived this study and designed the simulation. XC.H. and M.L. performed the simulation. XC.H., M.L., F.X. and ZG.Q. analyzed the data and wrote the manuscript. All authors contributed to the interpretation and discussion of the results.

Acknowledgements

This work was partially supported by the National Natural Science Foundation of China (51322604, 51176149, and 11372243), the Major International Joint Research Program of China (11120101002), and the International Science & Technology Cooperation Program of China (2013DFG02930).

References

1 Y. Cheng, L. Zhao, Y. Li and T. Xu, *Chem. Soc. Rev.*, 2011, **40**, 2673–2703.
2 R. Duncan and R. Gaspar, *Mol. Pharmaceutics*, 2011, **8**, 2101–2141.
3 S. Nie, *Nanomedicine*, 2010, **5**, 523–528.
4 S. Svenson, *Eur. J. Pharm. Biopharm.*, 2009, **71**, 445–462.
5 R. K. Jain and T. Stylianopoulos, *Nat. Rev. Clin. Oncol.*, 2010, **7**, 653–664.
6 J. J. Khandare, S. Jayant, A. Singh, P. Chandna, Y. Wang, N. Vorsa and T. Minko, *Bioconjugate Chem.*, 2006, **17**, 1464–1472.
7 R. Tong, L. Yala, T. M. Fan and J. Cheng, *Biomaterials*, 2010, **31**, 3043–3053.
8 K. M. Huh, S. C. Lee, Y. W. Cho, J. Lee, J. H. Jeong and K. Park, *J. Controlled Release*, 2005, **101**, 59–68.
9 W.-d. Tian and Y.-q. Ma, *Soft Matter*, 2012, **8**, 6378.
10 M. J. Cloninger, *Curr. Opin. Chem. Biol.*, 2002, **6**, 742–748.
11 V. Jain and P. V. Bharatam, *Nanoscale*, 2014, **6**, 2476–2501.
12 Y. Cheng and T. Xu, *Eur. J. Med. Chem.*, 2008, **43**, 2291–2297.
13 L. Monticelli, E. Salonen, P. C. Ke and I. Vattulainen, *Soft Matter*, 2009, **5**, 4433.
14 A. Akesson, C. V. Lundgaard, N. Ehrlich, T. G. Pomorski, D. Stamou and M. Cardenas, *Soft Matter*, 2012, **8**, 8972–8980.
15 Z.-l. Li, H.-m. Ding and Y.-q. Ma, *Soft Matter*, 2013, **9**, 1281.
16 A. J. Verkleij, R. F. A. Zwaal, B. Roelofsen, P. Comfurius, D. Kastelijn and L. L. M. van Deenen, *Biochim. Biophys. Acta, Biomembr.*, 1973, **323**, 178–193.
17 X. He, Z. Qu, F. Xu, M. Lin, J. Wang, X. Shi and T. Lu, *Soft Matter*, 2014, **10**, 139–148.
18 Z. G. Qu, X. C. He, M. Lin, B. Y. Sha, X. H. Shi, T. J. Lu and F. Xu, *Nanomedicine*, 2013, **8**, 995–1011.
19 J. Wang, Y. Wei, X. Shi and H. Gao, *RSC Adv.*, 2013, **3**, 15776–15782.
20 T. Yue, X. Zhang and F. Huang, *Soft Matter*, 2014, **10**, 2024–2034.
21 S. J. Marrink, A. H. de Vries and A. E. Mark, *J. Phys. Chem. B*, 2004, **108**, 750–760.
22 H. Lee and R. G. Larson, *J. Phys. Chem. B*, 2008, **112**, 7778–7784.
23 H. Lee and R. G. Larson, *J. Phys. Chem. B*, 2006, **110**, 18204–18211.
24 W.-d. Tian and Y.-q. Ma, *Soft Matter*, 2012, **8**, 6378–6384.
25 P. K. Maiti, T. Çağın, S.-T. Lin and W. A. Goddard, *Macromolecules*, 2005, **38**, 979–991.
26 I. Lee, B. D. Athey, A. W. Wetzel, W. Meixner and J. R. Baker, *Macromolecules*, 2002, **35**, 4510–4520.
27 L. X. Peng, A. Ivetac, A. S. Chaudhari, S. Van, G. Zhao, L. Yu, S. B. Howell, J. A. McCammon and D. A. Gough, *Biopolymers*, 2010, **93**, 936–951.
28 J. Lin, H. Zhang, Z. Chen and Y. Zheng, *ACS Nano*, 2010, **4**, 5421–5429.
29 P. V. Escriba, J. M. Gonzalez-Ros, F. M. Goni, P. K. Kinnunen, L. Vigh, L. Sanchez-Magraner, A. M. Fernandez, X. Busquets, I. Horvath and G. Barcelo-Coblijn, *J. Cell. Mol. Med.*, 2008, **12**, 829–875.
30 A. A. Gurtovenko, J. Anwar and I. Vattulainen, *Chem. Rev.*, 2010, **110**, 6077–6103.
31 R. D. Porasso, W. F. Drew Bennett, S. D. Oliveira-Costa and J. J. López Cascales, *J. Phys. Chem. B*, 2009, **113**, 9988–9994.
32 Y. Li, X. Chen and N. Gu, *J. Phys. Chem. B*, 2008, **112**, 16647–16653.
33 U. Essmann, L. Perera, M. L. Berkowitz, T. Darden, H. Lee and L. G. Pedersen, *J. Chem. Phys.*, 1995, **103**, 8577–8593.

Published on 27 July 2015. Downloaded by Xian Jiaotong University on 31/05/2016 08:36:03.

34 G. M. Torrie and J. P. Valleau, *J. Comput. Phys.*, 1977, **23**, 187–199.
35 S. Kumar, J. M. Rosenberg, D. Bouzida, R. H. Swendsen and P. A. Kollman, *J. Comput. Chem.*, 1992, **13**, 1011–1021.
36 D. Van Der Spoel, E. Lindahl, B. Hess, G. Groenhof, A. E. Mark and H. J. C. Berendsen, *J. Comput. Chem.*, 2005, **26**, 1701–1718.
37 W. Humphrey, A. Dalke and K. Schulten, *J. Mol. Graphics*, 1996, **14**, 33–38, DOI: 10.1016/0263-7855(96)00018-5.
38 W.-D. Tian and Y.-Q. Ma, *Soft Matter*, 2012, **8**, 2627.
39 W. Gao, J. M. Chan and O. C. Farokhzad, *Mol. Pharmaceutics*, 2010, **7**, 1913–1920.
40 C. Bechara and S. Sagan, *FEBS Lett.*, 2013, **587**, 1693–1702.
41 A. Verma and F. Stellacci, *Small*, 2010, **6**, 12–21.
42 X. C. He, M. Lin, F. Li, B. Y. Sha, F. Xu, Z. G. Qu and L. Wang, *Nanomedicine*, 2015, **10**, 121–141.
43 A. D'Emanuele and D. Attwood, *Adv. Drug Delivery Rev.*, 2005, **57**, 2147–2162.
44 O. Milhem, H. Mobedi, N. Day, N. McKeown, D. Attwood and A. D'Emanuele, *Polym. Mater.: Sci. Eng.*, 2001, **84**, 721.
45 M. Liu, K. Kono and J. M. J. Fréchet, *J. Polym. Sci., Part A: Polym. Chem.*, 1999, **37**, 3492–3503.
46 L.-Q. Xie, W.-D. Tian and Y.-Q. Ma, *Soft Matter*, 2013, **9**, 9319–9325.
47 S. J. Marrink and D. P. Tieleman, *Chem. Soc. Rev.*, 2013, **42**, 6801–6822.
48 W. F. D. Bennett and D. P. Tieleman, *J. Chem. Theory Comput.*, 2011, **7**, 2981–2988.